Traction Control of a Three-Wheeled Electric Motorcycle

Josef Nilsson

Henrik Sandstedt

LUND UNIVERSITY

Department of Automatic Control

MSc Thesis
TFRT-6138
ISSN 0280-5316

Department of Automatic Control
Lund University
Box 118
SE-221 00 LUND
Sweden

Printed in Sweden by Tryckeriet i E-huset
Lund 2021

Abstract

Traction control is a widely used control system to increase stability and safety of four-wheeled vehicles. The company OMotion AB develops and builds three-wheeled electric vehicles. With a new model in development they want to increase the safety. This thesis presents the work of developing and implementing a Traction Control System (TCS) for that new model.

Previously, a thesis work had been done at OMotion that implemented a slip control system for the longitudinal dynamics [Karlin, 2021]. It detected slip of the rear wheel and limited the torque to regain grip. However, the controller does not handle lateral slip. When cornering and pushing the throttle too hard the rear wheel can lose grip and oversteer, potentially resulting in a serious accident. By measuring the speed of the vehicle and the steering wheel angle, a desired yaw rate is obtained. This is compared to the actual yaw rate of the vehicle, giving a yaw-rate error which the feedback controller acts on.

To investigate the behavior of the vehicle with different control strategies, a model was built in Matlab's Simulink. The model can simulate longitudinal and lateral dynamics together with the forces on the tires. The tire model used was the Dugoff tire model.

The simulation performed well and made it possible to test different control strategies before implementation and testing on the real vehicle. Tests showed that a less aggressive controller was needed due to the disturbances that a real non-ideal driving surface brings. After the controller was properly tuned, the TCS successfully prevents a driver from losing control when accelerating too aggressively in a corner.

Acknowledgements

We would like to thank our supervisors Björn Olofsson at the Department of Automatic Control at Lund University and Ola Svensson, founder and CEO of OMotion, for their assistance during the thesis work. A special thanks to Ola for giving us the opportunity to do our thesis at OMotion and for his extensive guidance in working with the motorcycle.

Contents

1

Introduction

Figure 1.1 Photograph of OMotion 2. Photo: Jakobsson Addemotion.

1.1 Background

OMotion AB is a company founded in Lund in 2013 that develops and builds fully electric three-wheelers. Their first model was OMotion ETR and they are now building their second model, OMotion 2, seen in Figure 1.1. In this second model some new safety systems were desirable, one of which was a Traction Control System (TCS) and this was the origin of this thesis. OMotion has developed their own Electronic Control Unit (ECU) with a microcontroller written in the programming language C, and this is where the TCS will be implemented.

1.2 Problem and goals

The problem that this thesis work aims to solve is when the rear-wheel driven three-wheeler is turning, the rear wheel can lose traction and start to slip laterally, i.e., the vehicle oversteers, while the driver is pushing the throttle. The goal is to reduce the risk of a serious oversteer happening and prevent the driver from making it worse. This is to be done by controlling the torque on the rear wheel.

Another goal, which ties in with the main goal, is to develop a simulation model of the vehicle, where different control systems can be tested without having to implement them on the real vehicle. An aspect that also will be investigated is what scenarios the TCS can handle and what scenarios it can not.

1.3 Pre-existing literature

Modeling

Vehicle dynamics and tire dynamics are subjects with a lot of pre-existing knowledge since it is so useful to many companies. Several different vehicle models, such as the single-track model with only one front and one rear wheel with just three degrees of freedom, to more complex models, are described in plenty of books and reports together with different tire models such as Dugoff, Magic formula, and Brush [Dugoff et al., 1969] [Rajamani, 2012] [Shekhar, 2017].

Control

Most modern cars have a TCS and/or Electronic Stability Control (ESC) so there is a lot of pre-existing literature. A TCS mainly helps with maintaining traction in the driven wheels during acceleration while an ESC is a more comprehensive system that increases vehicle stability and has the ability to handle more situations than a TCS.

In [Rajamani, 2012] three different types of ESC are described; differential braking, steer-by-wire, and active torque distribution. Differential braking means that different braking torques are applied on each wheel independently to control the yaw moment, steer-by-wire can change the driver's steering-angle input, and active torque distribution is similar to differential braking except that it can apply a driving torque instead of a braking torque on the wheels independently. The most commonly used type is differential braking, sometimes, but not often, combined with active torque distribution [Rajamani, 2012] [Jin and Liu, 2014].

Recently there have been implementations of ESCs in new electric vehicles. Separate control of in-wheel motors makes very effective stability control possible, since active torque distribution becomes much easier than in traditional internal combustion engine vehicles. This is explored in [Montani et al., 2020] and [Chen and Kuo, 2014]. Montani et al. control the yaw rate and side-slip angles by first calculating the expected values using a reference vehicle model, and then creating a

yaw torque using a type of Linear Quadratic Regulator (LQR). Chen and Kuo use a three-level control strategy, where the first level is an LQR to calculate a desired yaw torque, the second level is control allocation which distributes the longitudinal tire forces to create the yaw torque, and the third level is slip-ratio control at each wheel based on a combined-slip tire model. They use the individual in-wheel motors as actuators with both driving torque and regenerative braking, and in [Montani et al., 2020] they also modify the driver's steering wheel input.

1.4 Contributions to further knowledge

Although there was an abundance of information on vehicle and tire models, it was hard to find an actual implementation of a complete simulation based on these models so this thesis can help to give insight into how such a simulation tailored to traction control of three-wheeled electric vehicles can be implemented.

This thesis deals with quite a unique case where the vehicle has three wheels, is electrically driven, and the brakes can not be controlled from the ECU that this thesis work's programming is done on. This means that differential braking is not possible and, since the vehicle is rear-wheel driven by a single rear wheel, active torque distribution is not able to create a yaw moment and is therefore not a solution. Lastly, the vehicle is mechanically steered so a steer-by-wire solution is not possible. This is why the system developed in this thesis is called a TCS instead of an ESC, because the way it works is closer to a TCS than an ESC even though the situations it intervenes in is similar to an ESC. Because of all these limitations, the solution developed in this thesis is new in the sense that many other stability systems do not rely singularly on restricting the overall drive torque and the effectiveness of this system can be of interest for people in the future working with TCSs and ESCs, especially for three-wheeled vehicles.

1.5 Report disposition

This report first in Chapter 2 describes the theory behind the approach that was taken to solve the problem at hand. Then in Chapter 3 the different sensors and measurements used are explained. After this the driving simulation, Chapter 4, followed by the controller, Chapter 5, are detailed. Then in Chapter 6 the results are presented, succeeded by a discussion and a conclusion of the project in Chapters 7 and 8, respectively.

2

Theory

2.1 Vehicle axis system

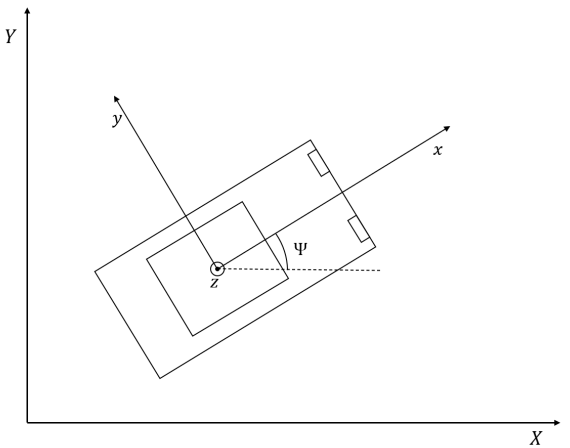

Figure 2.1 The vehicle axis system within the global coordinates

In this report, and in vehicle dynamics in general, the coordinate system used can be seen in Figure 2.1. The x-axis points in the forward, or longitudinal, direction of the vehicle. Pointing to the left of the vehicle, or the lateral direction, is the y-axis. The z-axis is pointing upwards and together with x and y they all intersect in the vehicle's Center of Gravity (CG). X and Y denote the global coordinates of the vehicle's CG. Ψ is the yaw angle of the vehicle, measured as the angle between X and x. A big focus of this report is on the yaw rate, the angular velocity around the z-axis, and it is denoted as $\dot{\Psi}$.

2.2 Coordinate calibration

A sensor making measurements along several axes is most likely not aligned with the desired coordinate system. It needs calibration and this can be done using a rotational matrix described by

$$R(\phi,\theta,\psi) = R_z(\psi)R_y(\theta)R_x(\phi) \tag{2.1}$$

where

$$R_x(\phi) = \begin{pmatrix} 1 & 0 & 0 \\ 0 & \cos\phi & -\sin\phi \\ 0 & \sin\phi & \cos\phi \end{pmatrix}$$
$$R_y(\theta) = \begin{pmatrix} \cos\theta & 0 & \sin\theta \\ 0 & 1 & 0 \\ -\sin\theta & 0 & \cos\theta \end{pmatrix}$$
$$R_z(\psi) = \begin{pmatrix} \cos\psi & -\sin\psi & 0 \\ \sin\psi & \cos\psi & 0 \\ 0 & 0 & 1 \end{pmatrix}$$

and ϕ, θ and ψ are the angles that the coordinate system is rotated around its x-, y-, and z-axis, respectively.

To determine what angles ϕ, θ and ψ would rotate the system correctly, two measurements of the accelerometer can be made. The first one is when the vehicle is standing completely leveled and the second one is when the rear is elevated. In the first measurement the values of $\ddot{x}$ and $\ddot{y}$ should be zero while $\ddot{z}$ should be g (gravitational acceleration) and in the second one $\ddot{y}$ should be zero. This is expressed in the function

$$f(\phi,\theta,\psi) = \begin{pmatrix} 0 \\ 0 \\ g \\ 0 \end{pmatrix} - \begin{pmatrix} R_{11} & R_{12} & R_{13} & 0 & 0 & 0 \\ R_{21} & R_{22} & R_{23} & 0 & 0 & 0 \\ R_{31} & R_{32} & R_{33} & 0 & 0 & 0 \\ 0 & 0 & 0 & R_{21} & R_{22} & R_{23} \end{pmatrix} \begin{pmatrix} \ddot{x}_{m1} \\ \ddot{y}_{m1} \\ \ddot{z}_{m1} \\ \ddot{x}_{m2} \\ \ddot{y}_{m2} \\ \ddot{z}_{m2} \end{pmatrix} \tag{2.2}$$

where the last vector is the measured values from the first and second measurement and the R-values are the matrix elements of the matrix R in Equation (2.1). The angles ϕ, θ and ψ that rotate the system correctly is obtained for

$$f(\phi,\theta,\psi) = \begin{pmatrix} 0 \\ 0 \\ 0 \\ 0 \end{pmatrix}$$

With the rotation matrix known, it is possible to calculate the accelerations and rotational velocities in the vehicle's coordinate system by

$$\begin{pmatrix} \ddot{x} \\ \ddot{y} \\ \ddot{z} \end{pmatrix} = R \begin{pmatrix} \ddot{x}_m \\ \ddot{y}_m \\ \ddot{z}_m \end{pmatrix} \tag{2.3}$$

$$\begin{pmatrix} \dot{\Phi} \\ \dot{\Theta} \\ \dot{\Psi} \end{pmatrix} = R \begin{pmatrix} \dot{\Phi}_m \\ \dot{\Theta}_m \\ \dot{\Psi}_m \end{pmatrix} \tag{2.4}$$

where the left-hand side is the values in vehicle coordinates and the right-hand side is the measured values.

2.3 Modeling

In this section the complete model is explained. First, the fundamental concepts of wheel dynamics, wheel slip angles and slip ratios are stated. Then the Dugoff tire model taken from [Dugoff et al., 1969] giving the tire forces is presented. From the tire forces, it is possible to obtain the accelerations of the vehicle using the vehicle body equations. In the last subsection (Global coordinates in simulation), it is shown how the global coordinates of the vehicle can be obtained from the accelerations. The equations are adapted to the OMotion 2, which is a three-wheeler with two wheels at the front and one at the rear, so for variables where the wheel needs to be specified; fl is "front left", fr is "front right" and r is "rear". The nomenclature for this section can be seen in Table 2.1.

Wheel dynamics

The angular accelerations from the longitudinal tire forces, braking torques and motor torque are described as

$$I_{wf}\dot{\omega}_{fl} = -\tau_{bfl} - r_f F_{xfl} \tag{2.5}$$

$$I_{wf}\dot{\omega}_{fr} = -\tau_{bfr} - r_f F_{xfr} \tag{2.6}$$

$$I_{wr}\dot{\omega}_r = \tau - \tau_{br} - r_r F_{xr} \tag{2.7}$$

Table 2.1 Nomenclature of Section 2.3 Modeling

I_{wf}	moment of inertia for a front wheel
I_{wr}	moment of inertia for the rear wheel
ω	angular velocity of a wheel
r_f	outer radius of a front wheel
r_r	outer radius of the rear wheel
F_x	longitudinal force on a tire
F_y	lateral force on a tire
F_z	normal force on a tire
τ	torque from motor acting on the rear wheel
τ_b	braking torque
α	slip angle of a wheel
δ	angle of a wheel
l_f	distance from CG to front axle
l_r	distance from CG to rear axle
l_w	distance between the front wheels' rotational axes
σ	slip ratio for a wheel
C_σ	tire longitudinal stiffness
C_α	tire cornering stiffness
μ	friction coefficient between tire and road
m	mass of the vehicle
I_z	vehicle's moment of inertia around z
F_{rr}	vehicle's rolling resistance
F_d	vehicle's air resistance

Wheel slip angles

The angle between the direction in which a wheel is moving and the direction it is pointed is calculated by [Shekhar, 2017]

$$\alpha_{fl} = \arctan\left(\frac{\dot{y}\cos\delta_{fl} + \dot{\Psi} l_f}{\dot{x}}\right) - \delta_{fl} \tag{2.8}$$

$$\alpha_{fr} = \arctan\left(\frac{\dot{y}\cos\delta_{fr} + \dot{\Psi} l_f}{\dot{x}}\right) - \delta_{fr} \tag{2.9}$$

$$\alpha_r = \arctan\left(\frac{\dot{y} + \dot{\Psi} l_r}{\dot{x}}\right) \tag{2.10}$$

This is illustrated in Figure 2.2, and the angles are called slip angles.

Slip ratios

The ratio between the difference in speed of the tire surface and the road surface passing, and the speed of the tire surface or the road surface depending on if the vehicle is accelerating or decelerating is described as [Rajamani, 2012]

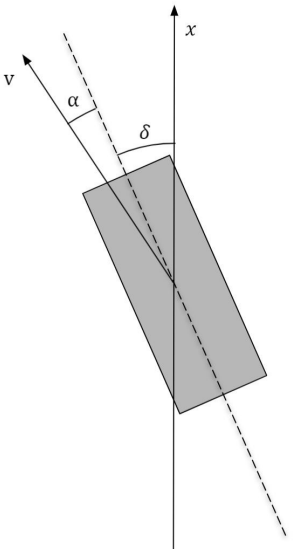

Figure 2.2 The slip angle α between the tire's velocity vector v and the direction it is pointing, the dotted line.

$$\sigma = \begin{cases} \frac{\omega r - \dot{x}}{\omega r}, & \omega r > \dot{x} \\ \frac{\omega r - \dot{x}}{\dot{x}}, & \omega r < \dot{x} \end{cases} \tag{2.11}$$

Dugoff tire model

The model used to derive the tire forces in this simulation is the Dugoff tire model [Dugoff et al., 1969]. It assumes an idealization of the contact region geometry between tire and road, where the pressure and deformation of the contact patch is uniform and the camber angle is zero.

This model first calculates the normalized longitudinal and lateral slip, $\bar{\sigma}$ and $\bar{\alpha}$ respectively, and the resultant of these, $\bar{\sigma}_r$, as

$$\bar{\sigma} = \frac{\sigma C_\sigma}{\mu F_z (1-\sigma)} \tag{2.12}$$

$$\bar{\alpha} = \frac{\tan(\alpha) C_\alpha}{\mu F_z (1-\sigma)} \tag{2.13}$$

$$\bar{\sigma}_r = \sqrt{\bar{\sigma}^2 + \bar{\alpha}^2} \tag{2.14}$$

This resultant is then used to calculate a normalized resultant tire force by

$$\frac{F_r}{\mu F_z} = \begin{cases} \bar{\sigma}_r, & \bar{\sigma}_r < 0.5 \\ \left(1 - \frac{1}{4\bar{\sigma}_r}\right), & \bar{\sigma}_r \geq 0.5 \end{cases} \tag{2.15}$$

The resultant tire force F_r is subsequently split into longitudinal and lateral tire forces as

$$F_x = \frac{\bar{\sigma}}{\bar{\sigma}_r} F_r \tag{2.16}$$

$$F_y = -\frac{\bar{\alpha}}{\bar{\sigma}_r} F_r \tag{2.17}$$

The tire forces saturate at higher slips, which is more realistic than for example a linear tire model, but not completely realistic since kinetic friction is lower than static friction and therefore in reality longitudinal tire forces would not only saturate but decrease when the wheels are close to locking.

Rolling resistance and air resistance

The rolling resistance for a tire is calculated by the formula $F_{rr} = C_r F_z$, where C_r is the rolling resistance coefficient [Rajamani, 2012]. Assuming that the sum of normal forces on the tires is $F_{z,total} = mg$ and that all tires have the same rolling resistance coefficient, it means that the total rolling resistance acting on the vehicle is

$$F_{rr} = C_r mg \tag{2.18}$$

The air resistance according to the drag equation is [Rajamani, 2012]

$$F_d = \frac{\rho \dot{x}^2 C_d A}{2} \tag{2.19}$$

where C_d is the drag coefficient, A is the frontal area of the vehicle and ρ is the density of air.

Vehicle body equations

Given the tire forces from the Dugoff tire model, it is possible retrieve the accelerations of the vehicle from [Rajamani, 2012]

$$\begin{aligned} m\ddot{x} = {} & F_{xfl}\cos\delta_{fl} + F_{xfr}\cos\delta_{fr} + F_{xr} - F_{yfl}\sin\delta_{fl} - F_{yfr}\sin\delta_{fr} + m\dot{\Psi}\dot{y} \\ & - F_{rr} - F_d \end{aligned} \tag{2.20}$$

$$m\ddot{y} = F_{xfl}\sin\delta_{fl} + F_{xfr}\sin\delta_{fr} + F_{yr} + F_{yfl}\cos\delta_{fl} + F_{yfr}\cos\delta_{fr} - m\dot{\Psi}\dot{x} \tag{2.21}$$

$$\begin{aligned} I_z\ddot{\Psi} = {} & l_f(F_{xfl}\sin\delta_{fl} + F_{xfr}\sin\delta_{fr}) + l_f(F_{yfl}\cos\delta_{fl} + F_{yfr}\cos\delta_{fr}) - l_r F_{yr} \\ & + \frac{l_w}{2}(F_{xfr}\cos\delta_{fr} - F_{xfl}\cos\delta_{fl}) + \frac{l_w}{2}(F_{yfl}\sin\delta_{fl} - F_{yfr}\sin\delta_{fr}) \end{aligned} \tag{2.22}$$

The normal forces of the tires are retrieved from

$$mg = F_{zfl} + F_{zfr} + F_{zr} \tag{2.23}$$

$$0 = \frac{F_{zfl} l_w}{2} - \frac{F_{zfr} l_w}{2} + F_{xfl}\sin(\delta_l)h + F_{xfr}\sin(\delta_r)h + F_{yfl}\cos(\delta_l)h + F_{yfr}\delta rh + F_{yr}h \tag{2.24}$$

$$0 = -F_{zfl} l_f - F_{zfr} l_f - F_{xfl}\cos(\delta_l)h - F_{xfr}\cos(\delta_r)h + F_{yfl}\sin(\delta_l)h + F_{yfr}\sin(\delta_r)h - F_{xr}h + F_{zr} l_r + F_{rr}\left(h - \frac{r_r + 2r_f}{3}\right) \tag{2.25}$$

All of these equations are derived from relating the forces acting on the vehicle to the accelerations of the vehicle using Newton's second law.

The left-hand sides of Equations (2.24)–(2.25) are moment of inertia multiplied with angular acceleration, and since the angular acceleration around the x- and y-axes in this model is assumed to be zero the results on the left-hand sides are also zero.

Equations (2.20)–(2.22) are then used to obtain the accelerations and integrate them to get the the velocities $\dot{x}$, $\dot{y}$ and $\dot{\Psi}$. The velocity $\dot{y}$ is changed slightly to be used in the calculation of global coordinates since the Equation (2.21) subtracts the centripetal force to calculate the acceleration away from the driving line. When calculating the global coordinates the centripetal force is therefore not subtracted, giving a velocity called $\dot{y}_{gc}$ integrated from

$$m\ddot{y}_{gc} = F_{xfl}\sin\delta_{fl} + F_{xfr}\sin\delta_{fr} + F_{yr} + F_{yfl}\cos\delta_{fl} + F_{yfr}\cos\delta_{fr} \tag{2.26}$$

Global coordinates in simulation

For visual representation of the vehicle's position and orientation when simulating, the global coordinates of the vehicle can be retrieved from the accelerations by

$$\Psi = \int \left[\int \ddot{\Psi} dt + \dot{\Psi}_0 \right] dt \tag{2.27}$$

$$X = \int \left[\int (\ddot{x}\cos\Psi - \ddot{y}_{gc}\sin\Psi)\, dt + \dot{x}_0 \right] dt \tag{2.28}$$

$$Y = \iint (\ddot{x}\sin\Psi + \ddot{y}_{gc}\cos\Psi)\, dt dt \tag{2.29}$$

2.4 Friction ellipse

In this section the concept of a friction ellipse is introduced, which together with simple vehicle dynamics will explain why limiting the driving torque can prevent a serious oversteer of the vehicle.

The friction ellipse is a way of describing the direction, size and limits of the friction between tire and road [Foale, 2006]. In Figure 2.3, the x-axis is in the longitudinal direction of the wheel and the y-axis is in the lateral direction. F is the friction force acting on the tire, it can be divided into F_x and F_y. The ellipse represents the maximum available friction in any direction. Generally, a tire is designed to give more lateral friction than longitudinal, hence the greater maximum friction along the y-axis. If trying to use more friction than the ellipse allows the wheel loses grip. When the wheel is slipping or spinning it would use maximum friction; F would be on the ellipse's border. This is a simplification as in most cases of friction between moving objects, the friction drops slightly compared to static friction. However, in explaining this concept that effect is negligible.

During slip of an object on a surface, the direction of the friction force acting on the object is in the opposing direction of the velocity with which the object is moving relative to the surface. In the tire–road case, the friction force acting on a purely spinning wheel would point in the positive x-direction and be as big as the ellipse allows. If the tire is slipping sideways to the right, the friction force would point in the positive y-direction and be as big as the ellipse allows.

As stated in Section 1.2 the problem that can arise when taking a corner is that the driver pushes the throttle too hard. In doing so the friction at the rear tire tries to go past the friction ellipse and the tire loses grip. Assume a left turn; losing grip at the rear, the vehicle starts to spin and the yaw rate $\dot{\Psi}$ increases. At this stage, the rear wheel's force is somewhere around F_1 on the friction ellipse in Figure 2.4, as the wheel is both spinning and slipping sideways. To stop the increase in yaw rate and the vehicle spinning out of control, it is desired to use as much friction force as possible from the rear wheel to oppose the now increasing yaw rate. This is done by maximizing the friction's y-component, giving a torque on the vehicle that counters the yaw rate. By decreasing the torque τ, and thus the spin of the wheel, the friction is brought from F_1 to F_2 in Figure 2.4. Now the torque around z can be enough to overcome the oversteer of the vehicle.

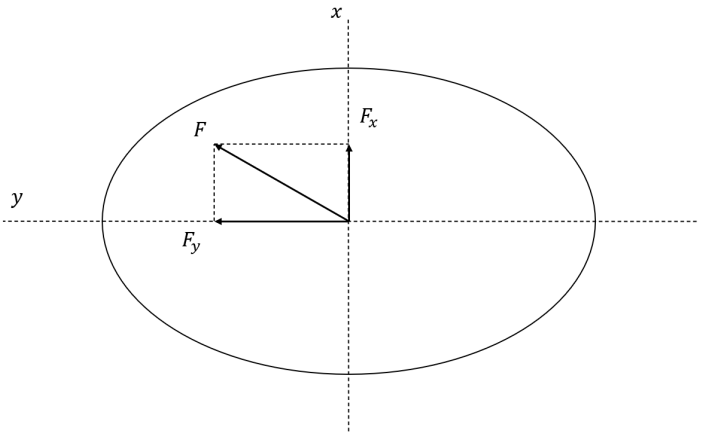

Figure 2.3 The friction ellipse.

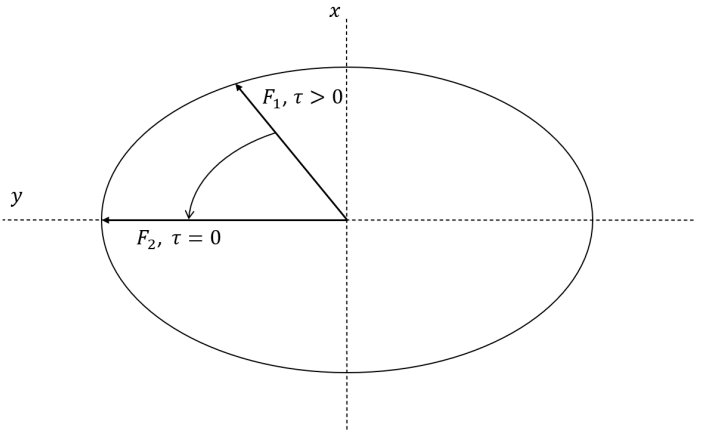

Figure 2.4 Friction force on the rear tire while oversteering. The force is F_1 when there is torque from the motor and the wheel is spinning and sliding. The force is F_2 when there is no torque and the wheel is only sliding sideways to the right.

3

Sensors and measurements

The sensors available for the vehicle were accelerometer, gyroscope, and potentiometer for the steering wheel angle. These sensors needed to be installed on the vehicle and this process is described in this chapter.

In addition to the sensors, several signals could be read from the vehicle's Controller Area Network (CAN) bus. The signals used in this thesis work were the motor's rotations per minute (rpm) and the motor's current. These were then converted to rear-wheel speed and rear-wheel torque, respectively. One quantity that is not measured in this project is the braking.

At the end of the project the first test vehicle of the model OMotion ETR was replaced by a new OMotion 2. In this new vehicle there was an Anti-lock Braking System (ABS) from which the front-wheel speeds could be extracted.

3.1 Accelerometer and gyroscope

The accelerometer and gyroscope were in the same inertial measurement unit mounted on the ECU. The accelerometer measured the acceleration in the unit's x-, y- and z-directions in milli-g, as in the gravitational acceleration, and this was then converted to mm/s^2. The gyroscope measured the rotational velocity around the three axes in millidegrees/s.

Since the ECU was mounted under the hood of the motorcycle in such a way that the coordinate system of the accelerometer/gyroscope did not align with the vehicle's coordinate system outlined in Figure 2.1, the measured values needed to be transformed into the vehicle's coordinate system. This was done according to the method described in the Section 2.2. The two measurements described in this method were done over a few seconds each and then the mean accelerometer values were used in the calculations. Since the accelerometer did not measure exactly g, the size of the total acceleration measured was calculated and used instead of g in Equation (2.2). The now slightly modified Equation (2.2) was then entered into the Matlab-function *fsolve*, that uses a least-squares solution. Since there are two solutions to $f = 0$, one with the x-axis pointing forward from the vehicle's perspec-

tive and one pointing backward, the right one has to be chosen. This was done by plotting a transformation of the vehicle's coordinate system and checking that it matched with the accelerometer's placement.

3.2 Steering

The steering was measured by mounting a potentiometer at the end of the steering column, converting the potentiometer's values to degrees and then calculating the wheels' angles based on this measured angle. The way this was calculated is described next.

Steering ratio

The steering ratio is the ratio between the steering wheel's turning angle and the wheels' turning angles. In the test vehicle that was used for the majority of this work, the steering ratio was slightly nonlinear and asymmetric. To be able to calculate the wheels' angles from the steering wheel's measured angle, measurements were made by hand which can be seen as cross marks in Figure 3.1. A third degree-polynomial curve was then fitted to these points using the Matlab-function *polyfit*, and these curves are seen as lines in Figure 3.1.

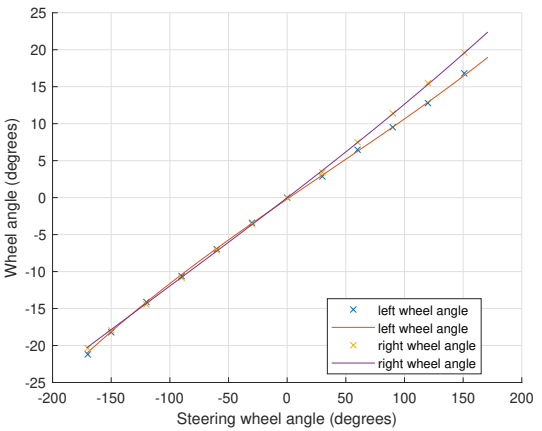

Figure 3.1 The measured wheel angles of the OMotion ETR and the polynomially fitted curve of wheel angles against the steering wheel angle on the horizontal axis.

At the end of the project the test vehicle was switched to the new OMotion 2 and therefore new steering measurements had to be made. These can be seen in Figure 3.2. In this new vehicle, the steering was not nearly as asymmetric as the previous one but there was still the problem of the outer wheel turning more than

the inner wheel in a left turn, although this was greatly reduced from the previous vehicle. In the future finished versions of OMotion 2 the steering will most likely be improved further and the steering will need to be mapped again.

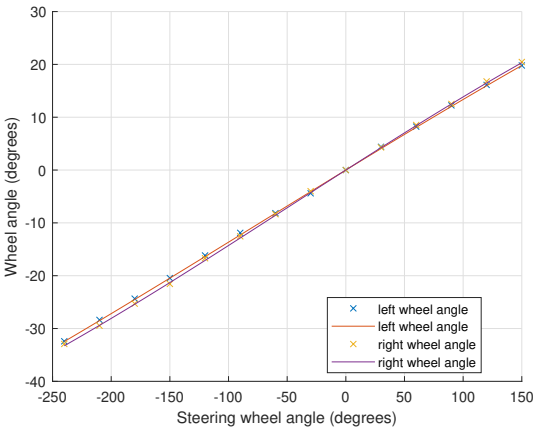

Figure 3.2 The measured wheel angles of the OMotion 2 and the polynomially fitted curve of wheel angles against the steering wheel angle on the horizontal axis.

3.3 Rear-wheel speed and applied torque

From the vehicle's CAN bus the motor's rpm and peak current were read and converted into rear-wheel speed and applied torque. Both of these conversions were done by simply multiplying with a factor. The current-to-torque factor was derived empirically, as described in Section 4.3. The rear-wheel speed was used as an estimation of the vehicle's speed in the first test vehicle.

3.4 Signal processing

The yaw-rate error signal to the controller, described in Section 5.1, and rear-wheel speed needed to be filtered through a low-pass filter to be more useful. The low-pass filter used was exponential smoothing

$$n(k) = \alpha m(k) + (1-\alpha)n(k-1) \tag{3.1}$$

where α is the smoothing factor, and $0 < \alpha < 1$.

In the case of the error signal, the smoothing factor used was $\alpha = 0.3$. This was done to prevent spikes in the signal to trigger the controller unnecessarily. The raw signal compared to the filtered signal is shown in Figure 3.3.

The rear-wheel speed was low-pass filtered for a different reason than the error. The low-pass filtering was mainly done to slightly delay a speed change and make too sudden of a change impossible. This was because the velocity that was actually desired was the vehicle's, not the driving wheel's, so the low-pass filtering of the speed made it a bit more realistic since there is always some slip on the tires, especially when there is a sudden change in speed. The speed signal can be seen in Figure 3.4.

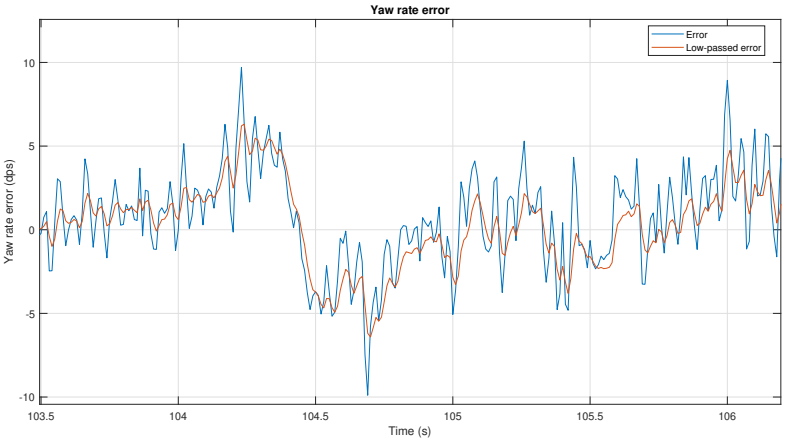

Figure 3.3 Plot of the yaw-rate error signal, both raw and filtered, during a drive test.

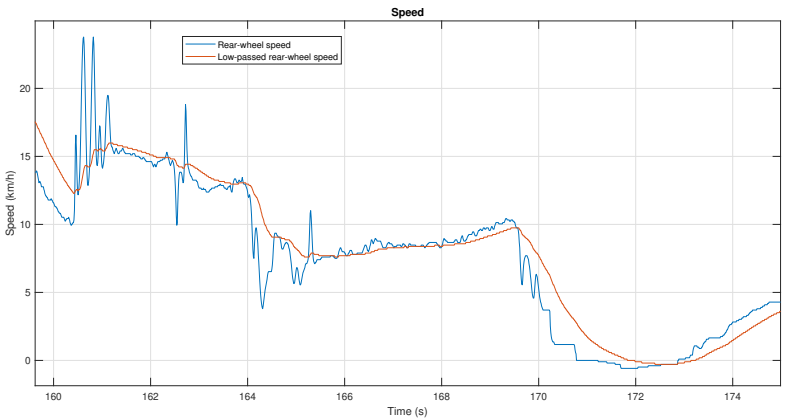

Figure 3.4 Plot of the rear-wheel speed, both raw and filtered, during a drive test.

3.5 Front-wheel speeds

To get the vehicle's speed, an average of the two front wheels' speeds was calculated. This measurement replaced the rear-wheel speed used in the previous vehicle since it was much more accurate due to the longitudinal slip at the rear wheel when accelerating since the front wheels are not driven.

4

Simulation

The simulation was made in Matlab's Simulink using the model from Section 2.3. It takes the steering wheel's angle and the motor current as inputs and from an initial state described by an initial speed and initial yaw rate, it then simulates the vehicle's behavior.

To check the accuracy of the simulation model and to tune the variables, several measurements were made of the yaw rate and speed during driving tests on the real vehicle where the inputs of motor current and steering angle were logged. When this was done, the logs of motor current and steering angle were fed into the simulation and the resulting yaw rate and speed graphs could be compared with the measured ones.

The values of C_α and C_σ was at first set the same values as used in [Shekhar, 2017] to verify that the tire model gave reasonable enough results to run the simulation. The rolling resistance and air resistance were initially set to zero and the current-to-torque factor was set to 0.5.

4.1 Simulink

Simulink [The MathWorks, Inc, 2021] is a modeling and simulation tool in Matlab which mainly uses customizable blocks to set up dynamical systems. This simulation used a fixed step size of 0.001 seconds and Simulink's automatic solver selection.

An overview of the Simulink model is shown in Appendix A. In Figure A.2 the subsystems are visible where all of the model parts described in Section 2.3 are implemented.

4.2 Rolling resistance and air resistance

To estimate the rolling resistance, air resistance and current-to-torque factor, a drive test was executed on the real vehicle where the driver first accelerated, then took the foot off the throttle and let the vehicle slow down by simply rolling. This test was

done on a flat area of asphalt, driving straight forward so as to not create additional resistance from the wheels. The vehicle is equipped with what is called a single-pedal drive system (SPD), which was disabled during this test run. This was because when lifting the foot off the throttle the SPD begins to charge the battery with the motor, braking the vehicle slightly. From the speed curve that was measured, the variables could then be derived by first calculating the rolling resistance from the slope of the curve when the vehicle was decelerating during the roll at the end. This slope is seen at the end of the graph in Figure 4.1.

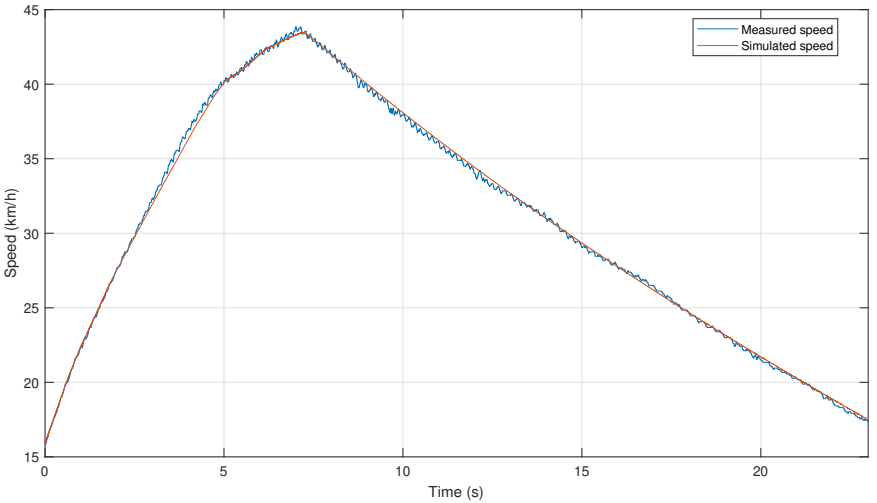

Figure 4.1 Vehicle's speed in km/h during acceleration and deceleration.

Assuming no air resistance, zero steering angle and no slip, C_r is derived from Equations (2.18) and (2.20) to be

$$C_r = \frac{-\ddot{x}}{g}$$

When this preliminary rolling resistance was calculated, a drag coefficient was estimated by manually changing it and also changing C_r so that the simulation's deceleration curve would fit with the measured one.

4.3 Current-to-torque factor

With the rolling and air resistances reasonably estimated the current-to-torque factor was estimated similarly to the drag coefficient, by iteratively changing it and looking at the acceleration part of the speed curve. The resulting simulated speed curve can be seen compared to the measured one in Figure 4.1.

4.4 Tire cornering and longitudinal stiffness

The variable C_α was changed from the initial values for the rear and front wheels separately to match the yaw rate of a driving test that included steering. This means that the simulation will be similarly under- or oversteered compared to the real vehicle. This was hard to get right since the steering on the test vehicle was asymmetric, see Figure 3.1, so the simulation's yaw rate fits better when steering to the right than to the left because in a left turn the right wheel has a comparably larger slip angle which is harder to simulate. This can be seen in Figure 4.2.

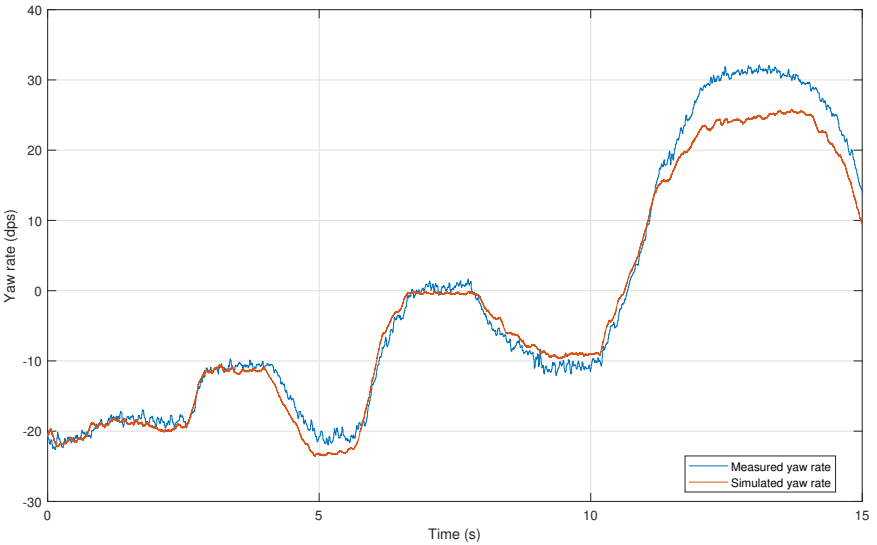

Figure 4.2 Yaw rate in degrees per second during a drive test with the first test vehicle.

The parameter C_σ was increased from the initial values to keep the ratio of $\frac{C_\sigma}{C_\alpha}$ close to the one used in [Shekhar, 2017].

5

Control

In this chapter all parts of the control system seen in Figure 5.1 are explained. An overview of sensors and actuator can be seen in Figure 5.2.

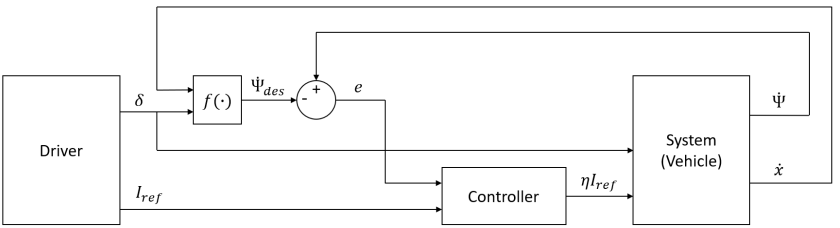

Figure 5.1 Block diagram of the controller connected to the vehicle.

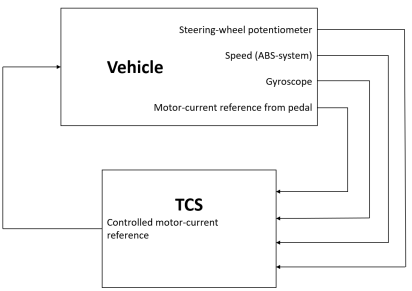

Figure 5.2 The vehicle and its sensors connected to the TCS with the controlled motor-current reference sent to the actuator on the vehicle.

5.1 Measurement signal and reference

The error input to the TCS's controller is in this implementation obtained by comparing the yaw rate $\dot{\Psi}$ (measurement signal) to a desired yaw rate $\dot{\Psi}_{des}$ (reference), as seen in Figure 5.1 and it is calculated by

$$e = \begin{cases} |\dot{\Psi}| - |\dot{\Psi}_{des}|, & \text{sgn}(\dot{\Psi}) = \text{sgn}(\dot{\Psi}_{des}) \\ |\dot{\Psi}| + |\dot{\Psi}_{des}|, & \text{sgn}(\dot{\Psi}) \neq \text{sgn}(\dot{\Psi}_{des}) \end{cases} \tag{5.1}$$

The actual vehicle yaw rate is measured by a gyroscope, while $\dot{\Psi}_{des}$ is calculated from the vehicle speed $\dot{x}$ and the front wheel's average angle δ.

The desired yaw rate is essentially the yaw rate the driver wishes to obtain at any moment. It takes into account the velocity of the vehicle, the angle of the steering wheel and the inherent under- or oversteer, much like the driver would. In [Rajamani, 2012] the desired yaw rate is stated as

$$\dot{\Psi}_{des} = \frac{\dot{x}}{R} = \frac{\dot{x}\delta_{ss}}{L + K_v \dot{x}^2} \tag{5.2}$$

Here, δ_{ss} is the the steady state steering angle for negotiating a circular road of radius R and it is calculated as

$$\delta_{ss} = \frac{L}{R} + K_v \dot{y} = \frac{L + K_v \dot{x}^2}{R} \tag{5.3}$$

The understeer gradient K_v is given by

$$K_v = \frac{l_r m}{2C_{\alpha f} L} - \frac{l_f m}{2C_{\alpha r} L} \tag{5.4}$$

where $C_{\alpha f}$ and $C_{\alpha r}$ are the cornering stiffnesses for the front and rear tires, respectively. However, this is for a car with four wheels. In the case of OMotion 2, which instead has one wheel in the rear, the equation becomes

$$K_v = \frac{l_r m}{2C_{\alpha f} L} - \frac{l_f m}{C_{\alpha r} L} \tag{5.5}$$

5.2 Controller

By multiplying the driver's current reference to the motor I_{ref} with a variable factor η ($0 \leq \eta \leq 1$) the control signal ηI_{ref} is obtained. Simulations made it clear that a fast response was needed when the rear wheel lost traction. When limiting the current reference gradually or too late, it was not possible to avoid a spin of the vehicle. From a driving-experience perspective it is desirable to interfere with the driver's inputs as little as possible, i.e., only engage the controller when e is large enough to

be sure there is a loss of traction. To protect the motor from damage, fast switching of the current reference between high and low values was to be avoided. Also, this vehicle will be driven in many different conditions, such as different surfaces and winds, conditions that can not be measured in this work. This calls for a limitation in complexity and number of tuning variables, as to not be affected too much by the varying conditions. With these abilities in mind, it was concluded that an on-off controller with hysteresis was best suited. The on-off controller can be seen in Figure 5.3. Here ε_2 is the value of e at which I_{ref} is set to zero and ε_1 is the value at which I_{ref} is again controlled by the driver.

Two variations of the on-off controller were also investigated and tested. The first one, an on-off controller with proportional start-up, is illustrated in Figure 5.4. The idea is that when the error is decreasing after loss of traction there should be a less abrupt engagement of the torque, which can decrease the risk of losing grip again because of too high torque. The second controller is an on-off controller just as seen in Figure 5.3 coupled in series with a time dependent increase of η. When the on-off controller is engaged and the error surpasses ε_1 the controller seen in Figure 5.5 takes over. Now η increases linearly from 0 to 1 over the time period from 0 to t_1. After t_1 the controller is disengaged. This approach is also meant to be more gentle in allowing the torque to again increase, but in addition makes the driver more aware that the controller has been activated and give time to decrease the pressure on the throttle.

Another aspect worth mentioning is the fact that the vehicle has SPD, so when the driver lifts the foot off the throttle the current reference does not go to zero but instead turns negative to slow the car down and use the kinetic energy to charge the battery. This braking leads to something called lift-off, which is load transfer between the wheels where the weight of the vehicle is transferred to the front wheels which reduces the amount of friction the rear wheel can generate. The motor braking also means that there is braking torque on the rear tire requiring longitudinal friction, which means that not all friction available goes in the lateral direction. This means that in the case of a spin-out, the best thing to do is to set the current reference to zero, applying no torque on the rear wheel, which the driver can not do by simply lifting the throttle. Therefore, the controller is required to do this since even if the driver would react as quickly as the controller, he or she can not disengage the single-pedal driving.

5.3 Implementation

In the ECU's microcontroller the current reference I_{ref} is passed to a function, along with speed of the vehicle, steering-wheel angle and yaw rate. In this function, the front wheels' angles are calculated from the steering-wheel angle with a third degree polynomial. The ECU calculates the desired yaw rate $\dot{\Psi}_{des}$ as Equation (5.2) presents. The yaw rate is compared to $\dot{\Psi}_{des}$ to give the error. The chosen controller

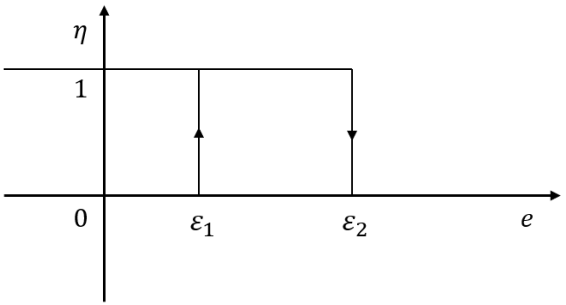

Figure 5.3 On-off controller with hysteresis

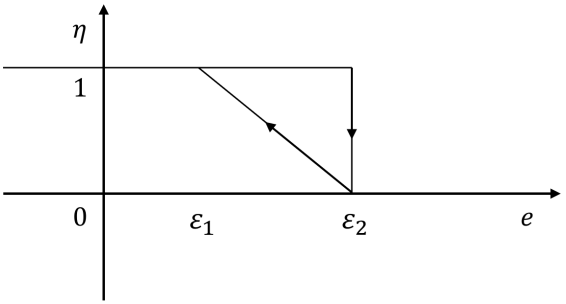

Figure 5.4 On-off controller with proportional start-up

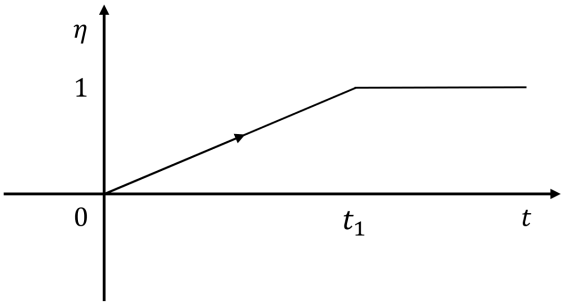

Figure 5.5 Time-dependent controller that can be coupled with the on-off controller

takes the error and gives an η which is between 1 (no limiting of the current reference) and 0 (current reference set to 0).

The implementation was made in steps to minimize mistakes and prevent dangerous behavior of the motor. After each step, a short test drive where logging of sensor and controller data were collected. The data could then be analyzed to investigate if there was any problem with the controller, otherwise further implementation could continue. The majority of the work was carried out on the OMotion ETR test vehicle, while the last few weeks an OMotion 2 was available and the controller was implemented on this as well.

6

Results

6.1 Simulation accuracy

The simulation's accuracy was tested by doing several test drives while logging the inputs and the measurements. The inputs were then fed into the simulation and the simulation's outputs were compared to the measurements. One of these drive tests' inputs are presented in Figure 6.1, and the comparison between the measurements and the simulation's outputs is seen in Figure 6.2.

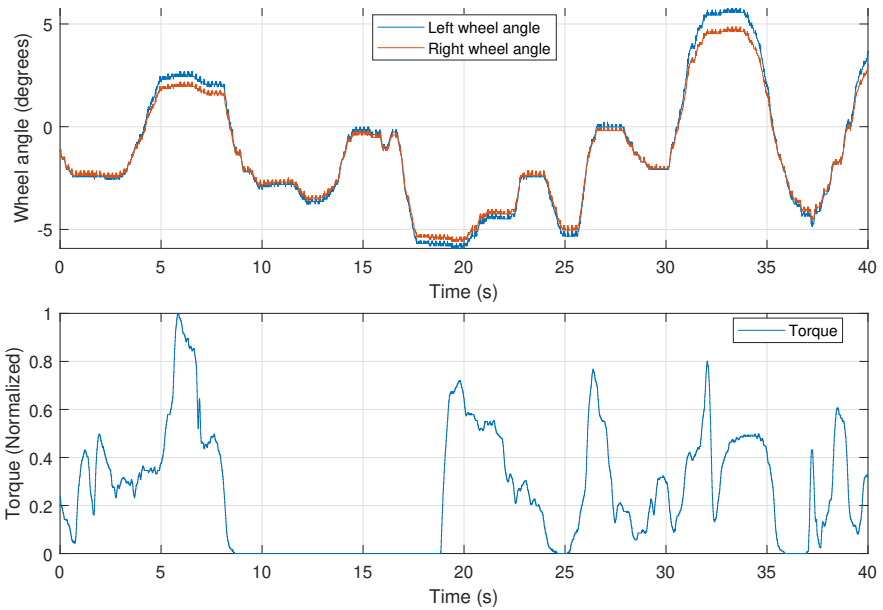

Figure 6.1 Steering and torque inputs during a test drive with the first test vehicle.

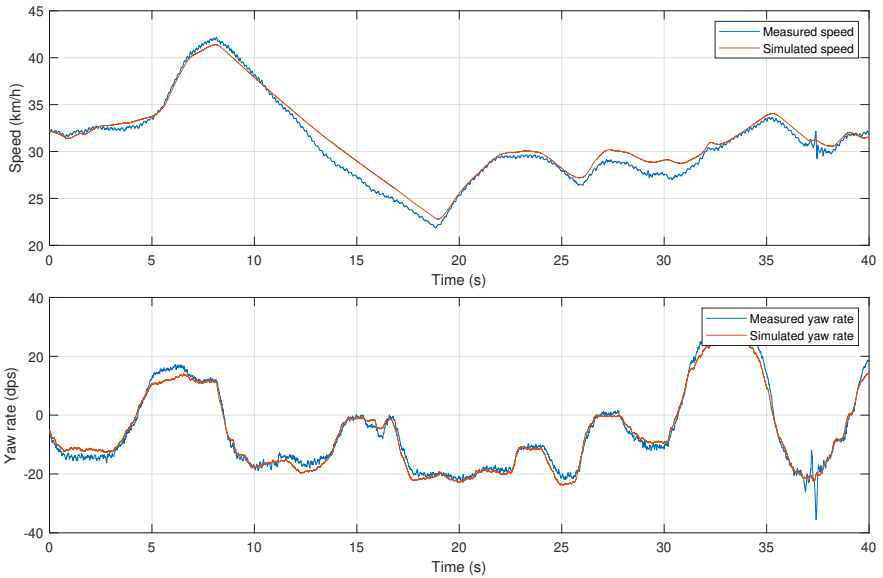

Figure 6.2 The simulated speed and yaw rate from the inputs in Figure 6.1 compared to the measured ones from a test drive with the first test vehicle.

6.2 On-Off Controller in simulation

To test the controller in the simulation environment, a drive test was simulated and additional torque was added during a turn until an oversteer was induced, to simulate too aggressive acceleration from the driver. Different values of ε_1 and ε_2 on the on-off controller were tested to see which performed the best. Several simulated oversteers using different ε_1 and ε_2 are shown in Figures 6.3–6.9. The figures show the simulated and the desired yaw rate to visualize the deviation, the rear-wheel slip angle, as well as the torque reference from the pedal and the applied torque from the controller. These values give insight into how severe the oversteer was.

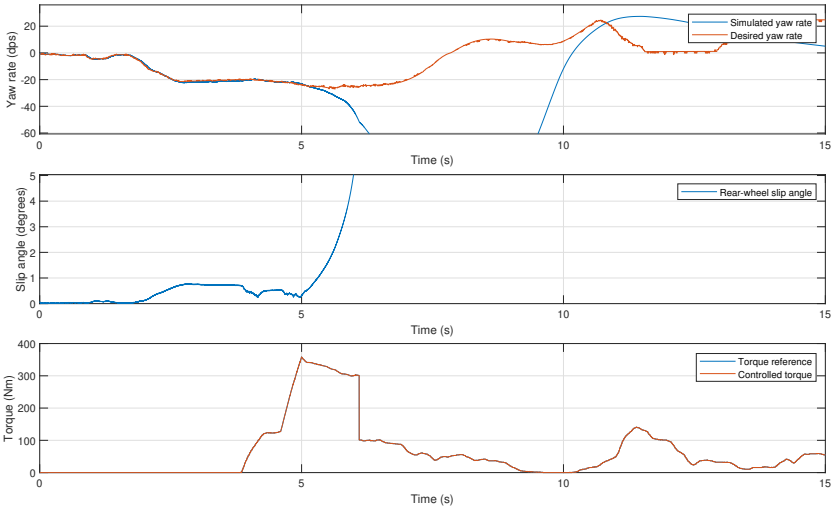

Figure 6.3 A simulated oversteer without any controller. The complete spin-out makes the slip angle and yaw rate grow uncontrollably outside the shown graphs.

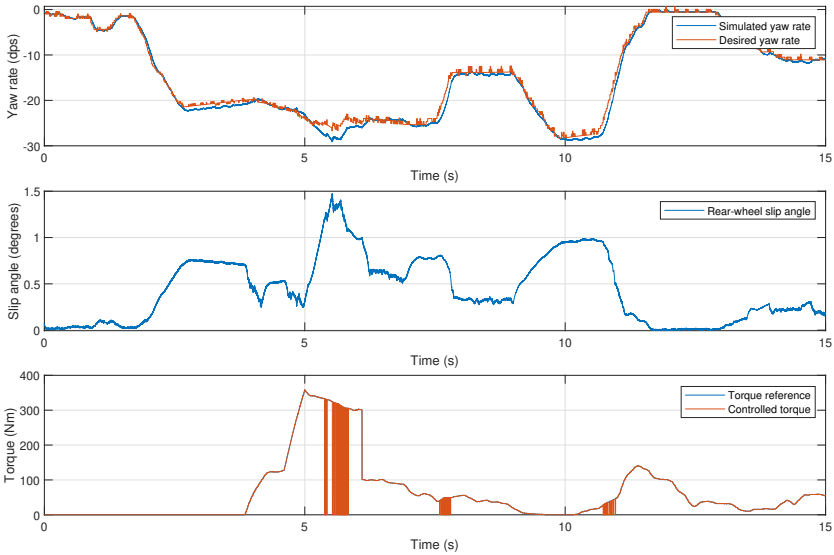

Figure 6.4 A simulated oversteer while the on-off controller was active, using $\varepsilon_1 = 3$ and $\varepsilon_2 = 3$, i.e., no hysteresis.

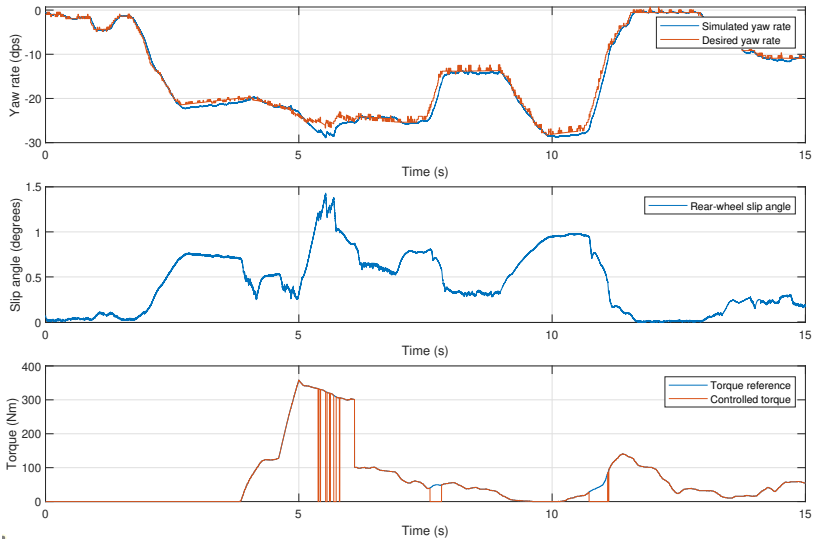

Figure 6.5 A simulated oversteer while the on-off controller was active, using $\varepsilon_1 = 2$ and $\varepsilon_2 = 3$.

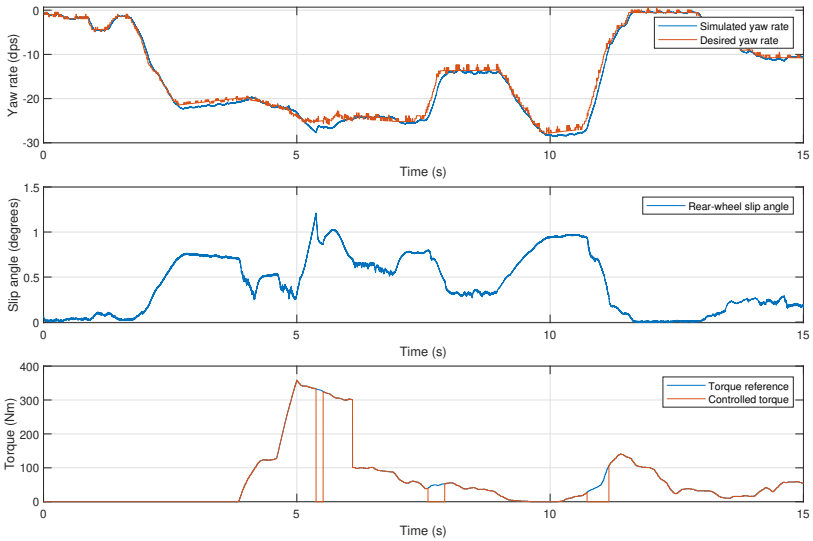

Figure 6.6 A simulated oversteer while the on-off controller was active, using $\varepsilon_1 = 1$ and $\varepsilon_2 = 3$.

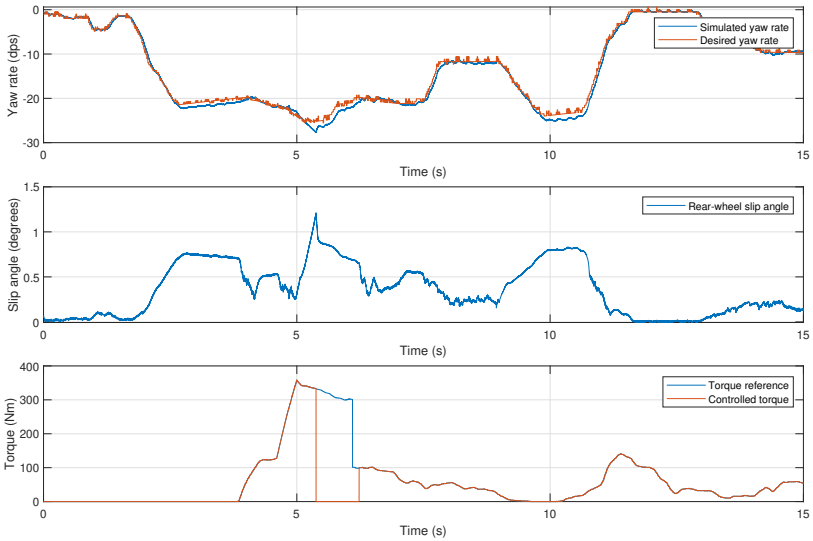

Figure 6.7 A simulated oversteer while the on-off controller was active, using $\varepsilon_1 = 0.5$ and $\varepsilon_2 = 3$.

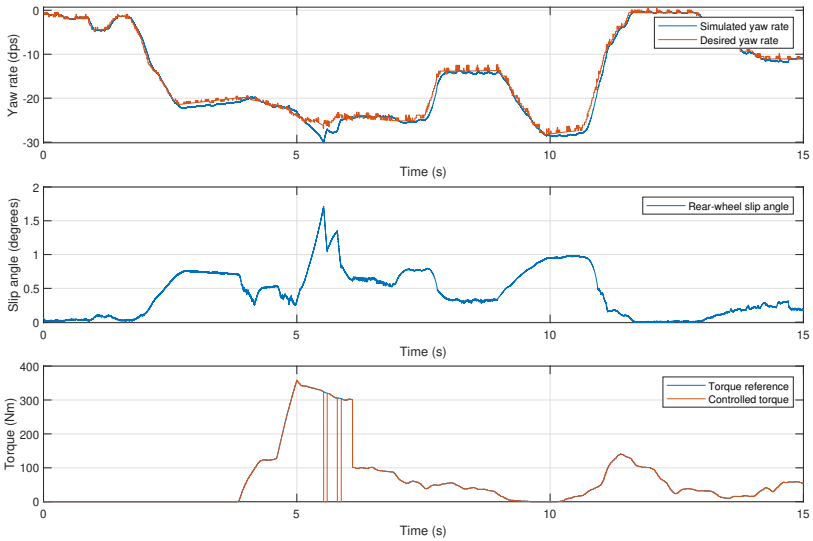

Figure 6.8 A simulated oversteer while the on-off controller was active, using $\varepsilon_1 = 1$ and $\varepsilon_2 = 4$.

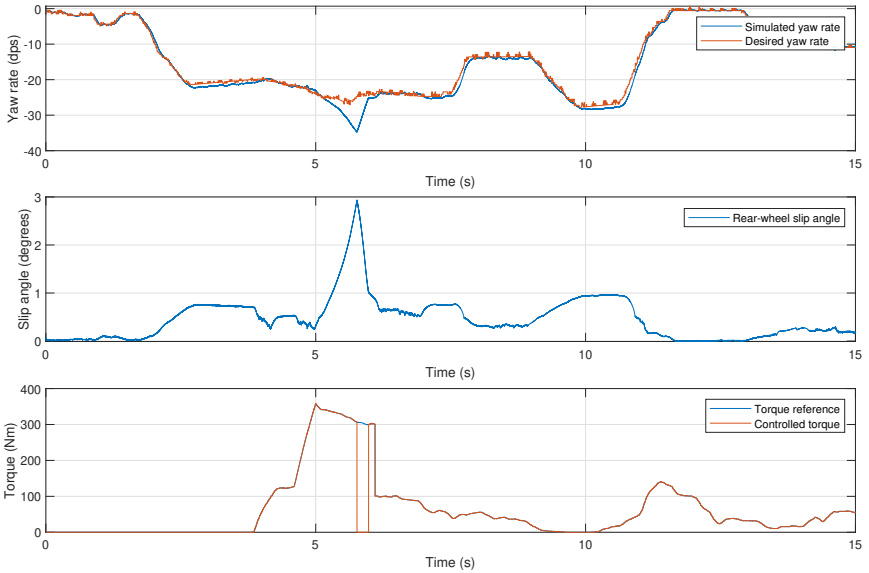

Figure 6.9 A simulated oversteer while the on-off controller was active, using $\varepsilon_1 = 1$ and $\varepsilon_2 = 10$.

6.3 On-Off Controller on the real vehicle

Figures 6.10–6.15 show oversteers performed at around 20 km/h on gravel with the real vehicle. The throttle was continuously pushed down through the oversteer to make it easy to analyze the effects of the controller.

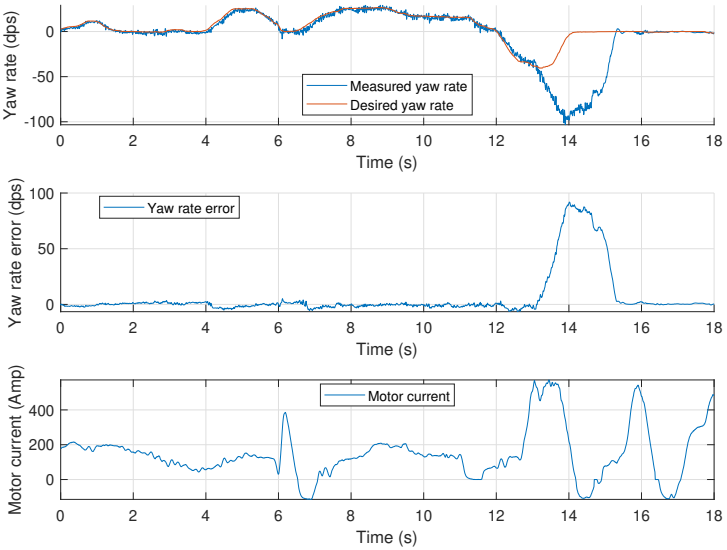

Figure 6.10 An oversteer on gravel without any controller.

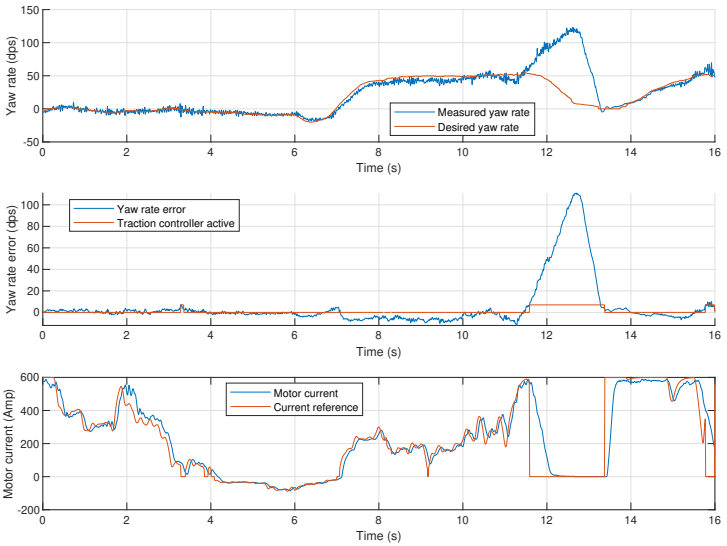

Figure 6.11 An oversteer on gravel while the on-off controller was active, using $\varepsilon_1 = 3$ and $\varepsilon_2 = 7$, but with a poorly tuned understeer gradient.

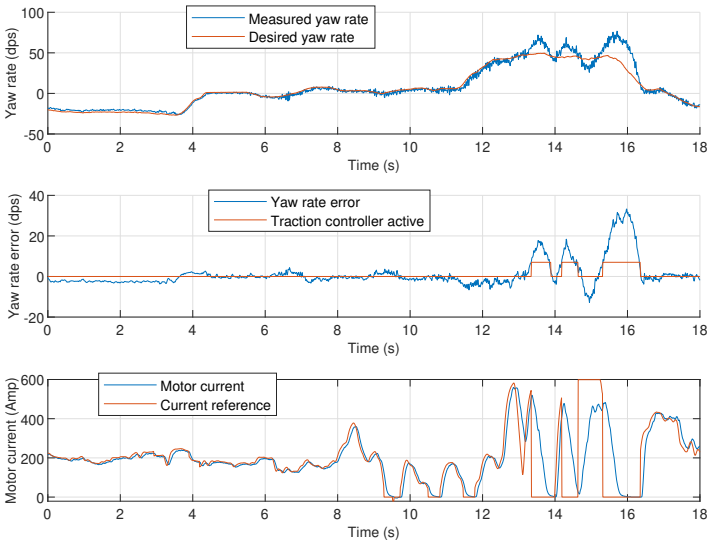

Figure 6.12 An oversteer on gravel while the on-off controller was active, using $\varepsilon_1 = 3$ and $\varepsilon_2 = 7$.

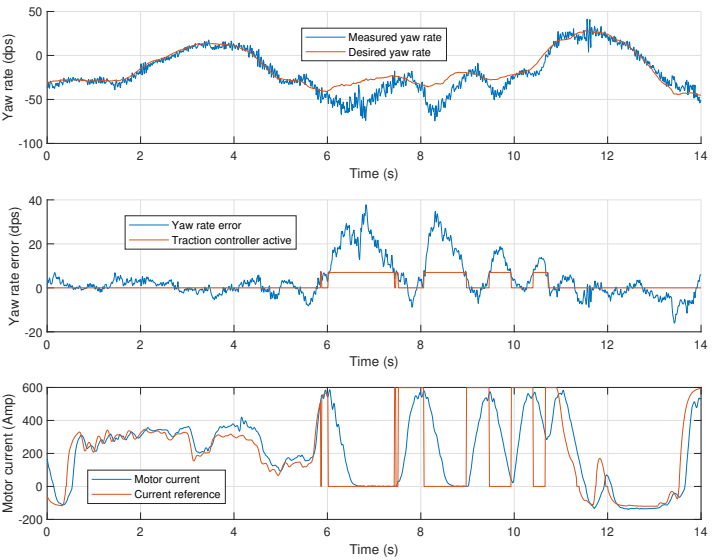

Figure 6.13 An oversteer on gravel while the on-off controller was active, using $\varepsilon_1 = 5$ and $\varepsilon_2 = 7$.

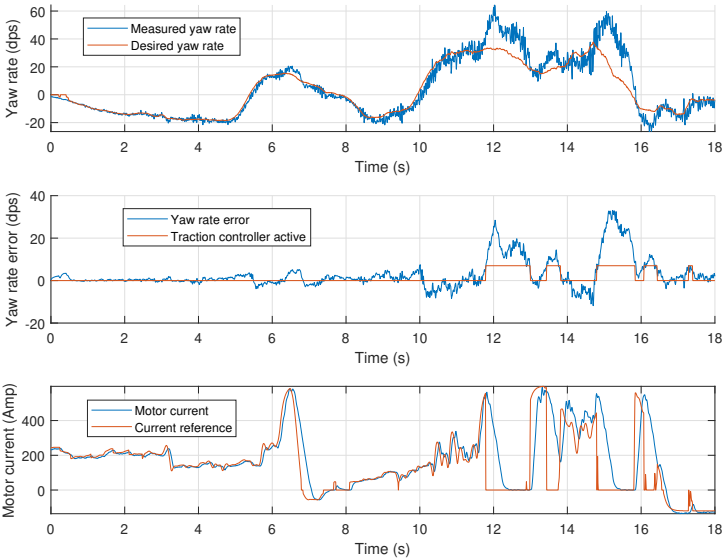

Figure 6.14 An oversteer on gravel while the on-off controller with proportional start-up was active, using $\varepsilon_1 = 3$ and $\varepsilon_2 = 7$.

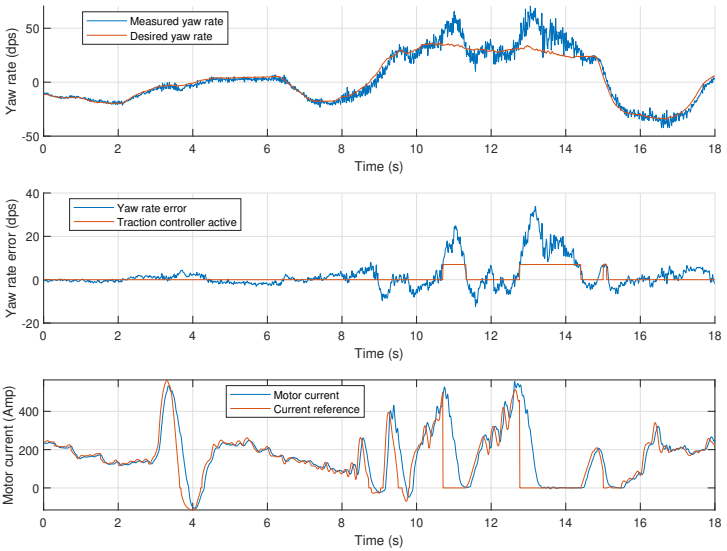

Figure 6.15 An oversteer on gravel while the on-off controller was active with a gradual start-up during one second, using $\varepsilon_1 = 3$ and $\varepsilon_2 = 7$.

7

Discussion

7.1 Controller simulations

In Figure 6.3 a simulated spin-out can be seen, caused by an excessive acceleration during a curve without any use of a controller. In Figures 6.4–6.9 the same driving is simulated but these times with an on-off controller with varying hysteresis parameters. The controller used in Figure 6.4 has no hysteresis and the result is a controller that turns on and off at a very high frequency during the slip, which might damage components in the motor. On the other end of the spectrum, there is the controller in Figure 6.7 with a wide hysteresis. The torque is only switched off once and is off for almost a second, maybe an unnecessarily long time because the yaw-rate error and slip angle are not significantly smaller than for the controller in Figure 6.6, which has the torque turned off for a fraction of the time. When comparing the controllers in Figures 6.5 and 6.6 it can be seen that the width of the hysteresis is important to not switch on and off at too high of a frequency and at the same time not limit the torque for too long. Comparing Figures 6.6 and 6.8 shows the importance of the size of the triggering error to not react to events that are not dangerous. Then looking at Figure 6.9, the cost of having a too large triggering error is seen by the large yaw-rate error and slip angle. These results give an idea for what aspects to have in mind when implementing the controller on the real vehicle.

Prior to the tested on-off controllers mentioned above, an attempt was made to use a form of PID controller. However, since the yaw-rate error grows so rapidly in an oversteer, this resulted in a PID controller that operated as an on-off controller in order to react quickly enough to actually prevent a severe oversteer. Since the PID controller was more complex than an on-off controller, but did not perform better, it was abandoned.

7.2 Experiments on the real vehicle

Figures 6.10–6.15 show the results of pushing the throttle while taking a curve on gravel. It was done on gravel due to the fact that when it was attempted with the test

vehicle on asphalt an oversteer could not be achieved because the rear wheel had too much grip, and the low speed was because of the limited space of the testing area. In Figure 6.10 there was no control and the result was that the vehicle rotated almost 180 degrees and faced the wrong direction when coming to a stand-still. This was the base line, with which the controllers could be compared to.

The first controller tested was the one used in Figure 6.11. This had little success as can be seen by comparing the yaw rates of this figure and the one with no control in Figure 6.10. The controlled vehicle eventually stopped rotating even though the foot was never taken off the throttle, but the vehicle had at this point rotated almost the same amount as in the uncontrolled case. The reason for this failure was determined to be an understeer gradient in the calculation of the desired yaw rate which did not reflect reality. This is visible in the yaw rate of Figure 6.11. The actual yaw rate is consistently below the desired one while driving the curve, which means that the controller will detect that there is an oversteer later than it should. This was fixed by increasing the understeer gradient until the desired yaw rate matched the measured one. This resulted in the controller used in Figure 6.12 which gave a much better result. This controller notices the oversteer early enough to prevent a serious oversteer like in Figure 6.10. It was not surprising that the understeer gradient calculated by Equation (5.5) was not completely accurate since the cornering stiffnesses were only roughly estimated. Also, in a real scenario the driver would probably feel the first oversteer and not continue to push full throttle, and thereby not continually return into an oversteer as was done in Figure 6.12; this was only done to demonstrate the effect of the controller.

Figure 6.13 shows a controller with $\varepsilon_1 = 5$ instead of 3 as in the previous controller. This was tested to see if the torque maybe could be applied sooner in the recovery. The result was that the motor current was switched on and off at a higher frequency which was not desirable, and the behavior of the vehicle was not better in any way.

The on-off controller with proportional start-up is shown in Figure 6.14. This shows that there is no point of doing this because the time window where the error is decreasing and also between ε_2 and ε_1 is so small that the current does not have time to change in a meaningful way.

The on-off controller with a gradual start-up over one second can be seen in Figure 6.15. This had the desired effect of making it harder to immediately go into another oversteer, but this could be achieved just as easily by the driver simply not pushing full throttle following the oversteer. Since lifting the throttle is the natural reaction, this did not really contribute to a safer or more comfortable driving experience. The experience was instead quite strange since the throttle did not give as strong of a torque as one expected, which resulted in pushing the throttle harder to compensate and eventually entering another oversteer anyway.

The vehicle is supposed to have a slip control system which limits the longitudinal slip at accelerations [Karlin, 2021]. This system should help with the problem of entering another oversteer when the throttle is turned on again since the longitudinal

slip is not allowed to increase so drastically and thereby reducing the lateral friction once more. However, this system was not functioning as intended while the test drives of this project were done and it is suspected that this was due to some issue with the ABS equipment and not with the actual controller. This is why there are no result graphs of the TCS and slip control working together. When the slip control is working as intended the idea is to feed the current reference in series from the TCS into the slip control, but as stated previously this could not be tested so the results of this combination of controllers are unknown at the moment of writing this report.

7.3 Performance of the simulation

The simulation was useful when trying out different control strategies. It is good at simulating the lateral and longitudinal dynamics. However, there are some limitations to how well it corresponds to reality. A perfectly level surface is assumed which can make comparisons between logged data and simulation difficult. Although, with a fairly flat test site this does not pose much problem. The values of C_α and C_σ are not provided by the tire manufacturer but are instead experimentally determined by comparing the logged data of the vehicle taking a corner to the same maneuver in the simulation. No logging of the brakes of the vehicle was possible and there is no implementation of brakes in the simulation. This is no problem when simulating a short sequence of maneuvers, but could limit investigation of other parts of the vehicle dynamics. As the slip angles and slip ratios include divisions by the speed of the vehicle $\dot{x}$ this becomes a problem in the simulation at very low speeds or no speed at all. In this case, the slips are given very large values and the simulation stops working. This is avoided by logical operators and starting the simulation with a starting speed not very close to zero. Perhaps what most limits the accuracy of the lateral dynamics is that there is no modeling of springs or dampeners connected to the wheels. This can have an impact on the tire forces when making quick changes in input, such as limiting the driving torque quickly.

When comparing the oversteer in the simulation and in reality, it is obvious that the simulation is not perfect when simulating an actual oversteer. The simulation has a more gradual increase of the error, which makes it easier to catch the vehicle in time and the error does not grow as large as in reality. Another aspect which makes reality harder to control is that the current, which also corresponds to the torque, does not follow the reference exactly. There is a delay in the real motor current which was not taken into account in the simulation. This means that the torque in reality is not reduced to zero instantly, making it harder to control the yaw rate since some of the friction will still be going into the longitudinal direction. The noise in the measured yaw-rate signal also makes reality harder to control because ε_2 could not be set as low as in the simulation, because of not wanting to trigger the controller unnecessarily.

7.4 Different scenarios for the controller

A goal of this work was to investigate what scenarios the controller can handle and which it can not. As seen in the results, loss of traction by taking a corner steadily and then pushing the throttle too hard is successfully avoided by the controller. This was the primary goal of this thesis, though it is also interesting to note what it can not do. Another way to initiate a loss of traction is by taking a corner steadily and then braking as to shift the majority of the weight to the front wheels. Without enough normal force on the rear wheel the motorcycle loses grip. This is called lift-off, and it could not be handled by the controller. This is because the driver is normally not able to react quickly enough to release the brake pedal and allow the rear wheel to help counter the now too high yaw rate. If turning into the corner too aggressively or by swerving back and forth it is also possible to lose traction. These scenarios can not be handled by the controller either, as the loss of traction is not caused by too much torque on the rear wheel and therefore the controller can not increase the lateral friction further.

7.5 Different surfaces

It is plausible that the controller will give different results on different surfaces, such as dry asphalt, wet asphalt, or dirt. Due to limited testing sites, these surfaces could not be tested. To implement the controller on these different surfaces, re-tuning of the controller parameters ε_1 and ε_2, as well as the understeer gradient K_v, is most likely required. Since the surface conditions are not measured in this thesis work, the driver would have to switch between these different controller parameters manually in some way. It might be possible to estimate the surface conditions by analyzing the yaw rate in real-time compared to the calculated desired yaw rate in a curve that is deemed to be safe by the algorithm to see if they are matching or if the driving surface has changed. This would however require a lot of work and it could be difficult to determine whether a curve was driven safely or not in real-time.

8

Conclusion and Future work

8.1 Conclusion

The controller that this thesis work recommends using is the on-off controller with hysteresis using $\varepsilon_1 = 3$ and $\varepsilon_2 = 7$. This limited the throttle early enough to prevent a severe oversteer and at the same time did not switch the motor current on and off too often. The experience when driving with this controller on is that it is significantly more difficult to spin out in an oversteer, but at the same time it does not feel like the performance of the vehicle is reduced or that the motor is limited at unnecessary times.

8.2 Future work

Several improvements could be done on the simulation. Firstly, the way that the actual motor current follows the current reference could be modified to more closely mimic the real motor. The cornering stiffnesses of the tires could also be investigated further to perhaps achieve a more realistic yaw-rate increase in an oversteer, and a more realistic tire dynamics overall. Lastly, measurement noise could be added to the simulated yaw-rate signal fed into the controller.

To improve the performance of this TCS in its ability to stabilize a vehicle, differential braking could be a possibility if the ECU was given control of the ABS-controlled brakes. This would transform the TCS into a full-fledged ESC and thereby increase the scenarios where it could be applied.

It is possible to make an implementation in the ECU of the Matlab-function *fsolve* that is more effective for this specific purpose. A convenient improvement that can be made is making the calibration of the gyroscope independent from Matlab-scripts and logging of sensor data to a computer. It would require some kind of input to the ECU to tell it when the vehicle is standing level and when the rear is elevated. However, this calibration should only need to be done once, when

the ECU is placed, and redone only if it is moved, so it is not a very high priority to simplify it.

The fact that the controller suggested in this work is tuned to driving on gravel limits the generality of it, since the vehicle is intended to be driven mostly on asphalt. Since it was not possible to oversteer on dry asphalt it might not be necessary to tune it to dry asphalt but it would be a good idea to tune it to wet asphalt. Then the driver could switch between the different modes depending on what the driving surface is. The TCS is also suggested to be tested at higher velocities than those used in this thesis' experiments to analyze how it performs under these conditions.

Gain scheduling of the controller could also be tested in the design to investigate if it gives better results. This was not tested since the test site only allowed for very similar test runs which would not give sufficient insight into if it made a difference or not.

Bibliography

Chen, B. and C. Kuo (2014). "Electronic stability control for electric vehicle with four in-wheel motors". *International Journal of Automotive Technology* **15**:4, pp. 573–580. DOI: 10.1007/s12239-014-0060-4.

Dugoff, H., P. S. Fancher, and L. Segel (1969). *Tire Performance Characteristics Affecting Vehicle Response to Steering and Braking Control Inputs*. Tech. rep. Highway Safety Research Institute at The University of Michigan, Ann Arbor, Michigan.

Foale, T. (2006). *Motorcycle Handling and Chassis Design*. 2nd ed. Tony Foale Designs. ISBN: 84-933286-3-4.

Jin, L. and Y. Liu (2014). "Study on adaptive slid mode controller for improving handling stability of motorized electric vehicles". *Mathematical Problems in Engineering* **2014**:1, pp. 1–10. DOI: https://doi.org/10.1155/2014/240857.

Karlin, A. (2021). *Slip Control for a Three-wheeled Electric Motorcycle*. MSc Thesis TFRT-6128. Department of Automatic Control, Lund University, Lund, Sweden.

Montani, M., T. Favilli, L. Berzi, R. Capitani, M. Pierini, L. Pugi, and C. Annicchiarico (2020). "ESC on in-wheel motors driven electric vehicle: Handling and stability performances assessment". *2020 IEEE International Conference on Environment and Electrical Engineering and 2020 IEEE Industrial and Commercial Power Systems Europe (EEEIC / I CPS Europe)* **2020**:1, pp. 1–6. DOI: 10.1109/EEEIC/ICPSEurope49358.2020.9160768.

Rajamani, R. (2012). *Vehicle Dynamics and Control*. Springer, New York Dordrecht Heidelberg London.

Shekhar, R. (2017). *Stability Analysis during Active Tire Excitation for Friction Estimation*. MSc Thesis 2017:26. KTH Royal Institute of Technology, Stockholm, Sweden.

The MathWorks, Inc (2021). *Simulink - Simulation and Model-Based Design - MATLAB & Simulink*. URL: `https://www.mathworks.com/products/simulink.html` (visited on 2021-06-10).

A

Simulink model

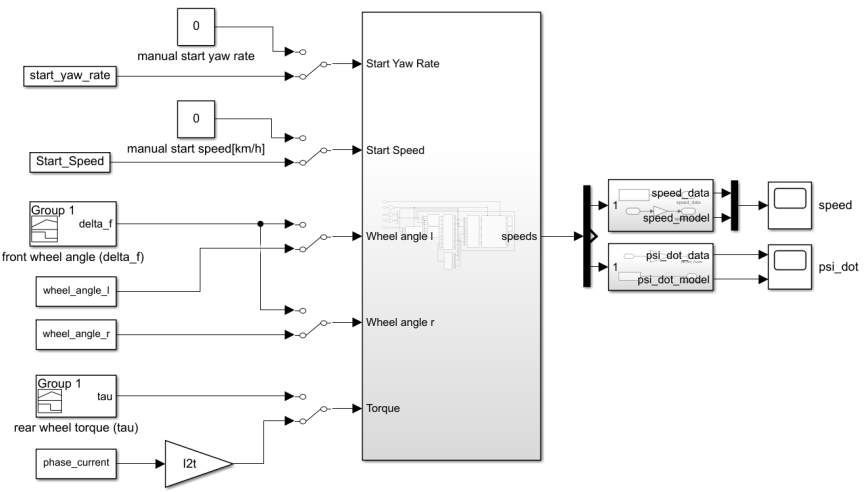

Figure A.1 The Simulink model with the inputs visible and in this case the switches are toggled to read data from the Matlab workspace. The subsystem in the middle is shown in Figure A.2.

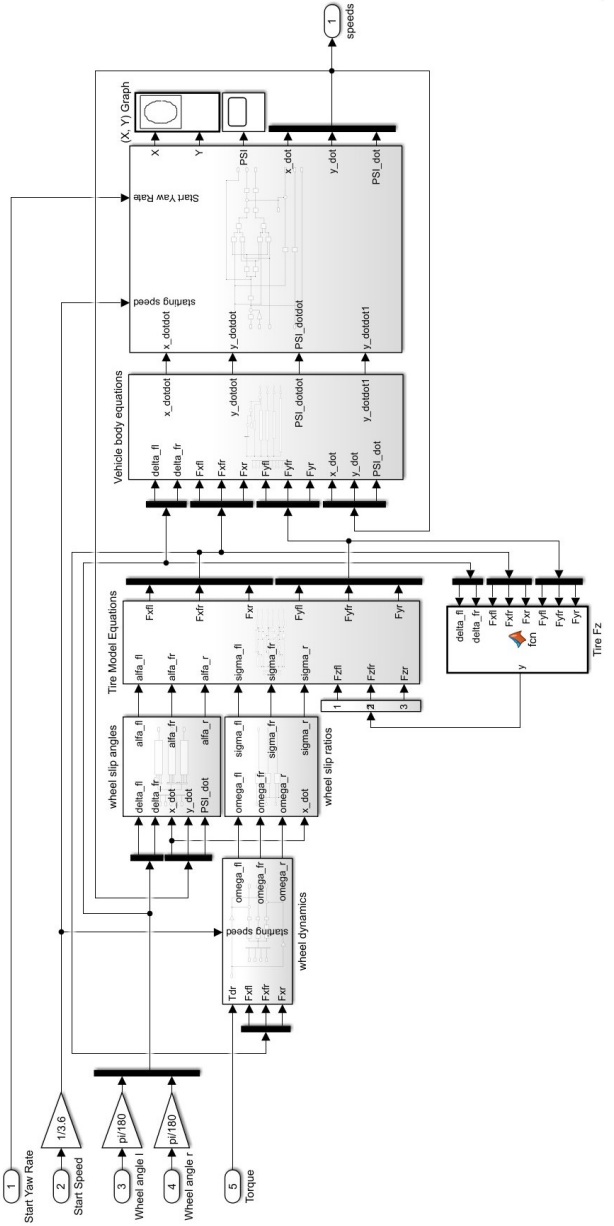

Figure A.2 The subsystem showing all of the subsystem blocks containing the model equations described in this report.

Lund University
Department of Automatic Control
Box 118
SE-221 00 Lund Sweden

Document name
MASTER'S THESIS

Date of issue
Aug 2021

Document Number
TFRT-6138

Author(s)
Josef Nilsson
Henrik Sandstedt

Supervisor
Ola Svensson, OMotion AB, Sweden
Björn Olofsson, Dept. of Automatic Control, Lund University, Sweden
Anders Robertsson, Dept. of Automatic Control, Lund University, Sweden (examiner)

Title and subtitle
Traction Control of a Three-Wheeled Electric Motorcycle

Abstract

Traction control is a widely used control system to increase stability and safety of four-wheeled vehicles. The company OMotion AB develops and builds threewheeled electric vehicles. With a new model in development they want to increase the safety. This thesis presents the work of developing and implementing a Traction Control System (TCS) for that new model.

Previously, a thesis work had been done at OMotion that implemented a slip control system for the longitudinal dynamics [Karlin, 2021]. It detected slip of the rear wheel and limited the torque to regain grip. However, the controller does not handle lateral slip. When cornering and pushing the throttle too hard the rear wheel can lose grip and oversteer, potentially resulting in a serious accident. By measuring the speed of the vehicle and the steering wheel angle, a desired yaw rate is obtained. This is compared to the actual yaw rate of the vehicle, giving a yaw-rate error which the feedback controller acts on.

To investigate the behavior of the vehicle with different control strategies, a model was built in Matlab's Simulink. The model can simulate longitudinal and lateral dynamics together with the forces on the tires. The tire model used was the Dugoff tire model.

The simulation performed well and made it possible to test different control strategies before implementation and testing on the real vehicle. Tests showed that a less aggressive controller was needed due to the disturbances that a real non-ideal driving surface brings. After the controller was properly tuned, the TCS successfully prevents a driver from losing control when accelerating too aggressively in a corner.

Keywords

Classification system and/or index terms (if any)

Supplementary bibliographical information

ISSN and key title
0280-5316

ISBN

Language
English

Number of pages
1-52

Recipient's notes

Security classification

http://www.control.lth.se/publications/